Mon. Not. R. Astron. Soc. **359,** 308–314 (2005) doi:10.1111/j.1365-2966.2005.08887.x

On the influence of relativistic effects on X-ray variability of accreting black holes

Piotr T. Życki[1]★ and Andrzej Niedźwiecki[2]

[1]*Nicolaus Copernicus Astronomical Centre, Bartycka 18, 00-716 Warsaw, Poland*
[2]*Łódź University, Department of Physics, Pomorska 149/153, 90–236 Łódź, Poland*

Accepted 2005 February 1. Received 2005 January 31; in original form 2004 September 17

ABSTRACT

X-rays produced by compact flares corotating with a Keplerian accretion disc are modulated in time by Doppler effects. We improve on previous calculations of these effects by considering recent models of intrinsic X-ray variability, and we compute the expected strength of the relativistic signal in current data of Seyfert galaxies and black hole binaries. Such signals can clearly be seen in, for example, recent *XMM–Newton* data from MCG–6-30-15, if indeed the X-rays are produced by corotating flares concentrated toward the inner disc edge around an extreme Kerr black hole. The lack of the signal in the data collected so far gives support to models where the X-ray sources in active galaxies do not follow Keplerian orbits close to the black hole.

Key words: accretion, accretion discs – relativity – galaxies: active – X–rays: binaries – X–rays: individual: MCG–6-30-15.

1 INTRODUCTION

Matter accreting on to compact objects (black holes, neutron stars) can be accelerated to relativistic velocities. The best observational evidence of such velocities comes from distortions of spectral features due to Doppler energy shifts. Some of the best evidence for relativistic motion in accreting black holes – in both active galactic nuclei (AGNs) and black hole binaries (BHBs) – is the broad Kα lines of Fe near 6.5 keV (see review in Reynolds & Nowak 2003). These can be explained by Doppler and gravitational energy shifts, from Keplerian motion of the emitting plasma, deep in the gravitational potential wells of the central objects.

Spectral distortions are not the only effect of relativistic motions of sources of radiation. The observed flux should be modulated in time, corresponding to periodic Doppler enhancement and reduction as the source revolves around the central body. The primary emission will be modulated, if its source also participates in the rapid Keplerian motion. We can thus expect periodic time modulation of the primary X-ray emission from accreting compact objects in those spectral states, when the emission is coming from magnetic flares. This applies to, for example, BHBs in soft states. Generally, such time modulation should be observed from sources showing broad Fe lines, again, under the assumption that the primary emission originates in magnetic flares rotating with the disc, rather than, for example, the base of a jet. The presence of a magnetically driven active corona is naturally expected from evolution of magnetic field inside an accretion disc (e.g. Galeev, Rosner & Vaiana 1979), and it is in fact supported by recent magnetohydrodynamical simulations (Turner 2004).

The purpose of this paper is to estimate the strength of the modulation in X-ray power density spectra (PDS) from accreting black holes. First computations of the appearance of a source orbiting a black hole were performed by Cunningham & Bardeen (1972) and Bardeen & Cunningham (1973). The influence of relativistic effects on time variability of accreting black holes was estimated by Abramowicz et al. (1991), and in subsequent papers by, for example, Bao (1992) and Bao & Ostgaard (1995). They assumed a collection of uncorrelated emitting hotspots, so the variability came in part from the emergence and disappearance of the hotspots, and in part from the relativistic effects. We are more specific in our approach as to the form of the intrinsic (i.e. before the relativistic effects) variability.

We assume that the basic form of variability PDS is realized without the relativistic effects (we use the flare avalanche model of Poutanen & Fabian 1999, hereafter PF99; see below). The latter give additional observable results. The motivation for formulating the basic model without relativistic effects is that the observed PDS has the basic form of (at least approximately) a doubly broken power law for many kinds and spectral states of accreting compact objects. This includes both the low/hard and high/soft states of black hole X-ray binaries, where the accretion flow geometries seem to be quite different, yet the power spectra are similar, at least in their high-frequency parts (see reviews in Done 2002; Zdziarski & Gierliński 2004). The X-ray power spectra of Seyfert galaxies have the same form, with break frequencies roughly scaling with central mass (Czerny et al. 2001; Markowitz et al. 2003). Also, the time-scales of broad-band X-ray variability in accreting compact systems are much

★E-mail: ptz@camk.edu.pl

longer than the Keplerian time-scales of the inner accretion disc, so other mechanisms of generating the variability must operate. We note that Miniutti & Fabian (2004) attribute much of the complex X-ray variability of MCG–6-30-15 specifically to Doppler and light bending effects from close to the central black hole. At the same time, Vaughan, Fabian & Nandra (2003) noticed similarity of power spectra, time lags and coherence function between MCG–6-30-15 and Cyg X-1, with a simple scaling with the black hole mass.

However, even though the basic variability model does not seem to require relativistic effects, these effects are quite clear in energy spectra of many sources. In extreme cases, model fits to the observed profiles of the Fe Kα line indicate that the emission must come from well within $6R_{\rm g}$, the marginally stable orbit in the Schwarzschild metric. This is claimed to be the case for Seyfert 1 galaxy MCG–6-30-15 (Fabian et al. 2002), and the BHBs, GX 339-4 (Miller et al. 2004) and XTE J1650-500 (Miller et al. 2002), where the estimated inner radii are $\approx$2–3$R_{\rm g}$. In addition, the radial emissivity of the line seems to be strongly peaked toward the inner radius. Thus, the relativistic effects should contribute to the variability characteristics, for example, the power spectra.

We adopt the flare avalanche variability model of PF99, and assign radial locations to the flares. We implement the relativistic effects in the extreme Kerr metric ($a = 0.998$), and compute the modulation in the observed X-ray light curves due to relativistic effects, as a function of inner disc radius and inclination angle. We compute the PDS, and demonstrate that for the extreme cases of inner radius being close to the marginally stable orbit ($R_{\rm ms} = 1.23R_{\rm g}$), the signal should be observed in current high-quality *XMM* data.

2 THE MODEL

2.1 Variability model and energy spectra

The model is very similar to that used by Życki (2002), and it is based on the variability model of PF99. The X-ray emission is assumed to be produced in the active region filled in with hot plasma, related to, for example, magnetic activity in the accretion disc corona. An active region produces a flare of radiation by inverse Compton upscattering of soft photons from the accretion disc. The soft photons, in turn, come mostly from reprocessing of the hard X-rays. The spectrum of emitted radiation evolves in time during the flare, from softer to a rather hard one close to the flare peak. This evolution can be caused by, for example, rising of the active region above the disc during the flare. The flares are correlated to produce longer 'avalanches', which help explain the f^{-1} part of the power spectrum (see PF99 for a detailed description). Compared to the original formulation of PF99, we modified the shape of the heating function, $l_{\rm h}(t)$, where $l \equiv (L/R_{\rm flare})(\sigma_{\rm T}/m_{\rm e}c^3)$ is the compactness parameter. It is assumed to be a double exponential function with the rise time much longer than the decay time, $\tau_{\rm r} \gg \tau_{\rm d}$, based on the autocorrelation and cross-correlation analyses by Maccarone, Coppi & Poutanen (2000). The rise time-scales of the flares are distributed between $\tau_{\rm min}$ and $\tau_{\rm max}$ with the distribution $P_\tau(\tau) \propto \tau^{-p}$ (see PF99). The cooling of the hot plasma is by soft disc photons from reprocessed X-rays, $l_{\rm s}(t) \equiv l_{\rm h}(t)\ D(t)$, and the feedback function, $D(t)$, is defined as in PF99.

We note that the model of PF99 was originally formulated for the hard/low state of BHBs, where the PDS has the characteristic shape of a doubly broken power law. Power spectra in the soft state have a different form, because the low-frequency break (from f^0 to f^{-1}) is not observed (Cyg X-1, Churazov, Gilfanov & Revnivtsev 2001; NGC 4051, McHardy et al. 2004), at least down to frequency $\approx 10^{-5} \times f_{\rm h,br}$, where $f_{\rm h,br}$ is the high break frequency. Also, the shape of the break in the soft state PDS is more gradual than in the hard state. However, these differences do not affect our reasoning and computations, because the considered effects appear on the f^{-2} part of the PDS, i.e. past the high-frequency break. This part of the PDS is formed by superposition of Fourier transforms of individual flare profiles and, as such, depends on properties of individual flares and distribution of their lifetimes. We also note that in the extreme soft state of Cyg X-1 the rollover frequency seems to be similar to that in the hard state (fig. 4 in Zdziarski & Gierliński 2004), i.e. there seems to be no difference in the PDS extent between the hard and soft states in Cyg X-1.

Flares are assumed to follow Keplerian orbits, starting from a randomly selected azimuthal location, so that the primary emission is modulated by the relativistic and kinematic effects. The vertical velocity of a rising plasma region (PF99), $v_{\rm z}$, is usually much smaller than the Keplerian velocity,

$$\frac{v_{\rm z}}{v_\phi} = \frac{H}{R}\frac{1}{\Omega_{\rm K}\tau_{\rm fl}}, \qquad (1)$$

(where H is the height above the disc of the point of flare's maximum luminosity) because $H/R \ll 1$. Therefore, we neglect the vertical motion while computing the Doppler effects. For the purpose of computing the relativistic effects, we assume that the emission comes from the equatorial plane.

The crucial model assumption is the radial distribution of flares. A steep centrally peaked distribution obviously enhances the importance of relativistic effects, while a flatter distribution makes these effects less important. We assume here that the flares are distributed in such a way that the energy emitted in X-rays follows the prescription for gravitational energy release in extreme Kerr metric, $Q(r)$ (see, for example, Krolik 1999, p. 152). The steep emissivity is also motivated by the results of fitting the observed profile of the Fe Kα line, which in some cases indicates very steep and centrally peaked emissivity (Fabian et al. 2002; Miller et al. 2002, 2004). The above assumption of emissivity is an important change compared to our previous model (Życki 2002). There, the assumption was made that the radial location of a flare is related to its time-scale, $r \propto \tau_{\rm fl}^{2/3}$ derived from $\tau_{\rm fl} \propto \Omega_{\rm K}^{-1}$, as expected from numerical simulations (e.g. Romanova et al. 1998). However, this leads to contradictions with observations, because, with all the assumptions of the original model of PF99, the longer flares emit more energy than the short flares, yet they are located farther away from the centre (see Życki 2002, for a detailed discussion). Therefore, in the present model there is no relation between the flare time-scale and its location; we also discuss in Section 3.1 whether relaxing this assumption can modify our results. The radial position of a spontaneous flare is generated from probability distribution $P_r(r) \propto rQ(r)$ (corresponding to energy dissipation per ring), and all the flares stimulated by a given spontaneous flare are located at the same radius.

At each moment of time, the energy spectrum is computed. We approximate the Comptonization spectrum as the sum of a power law with exponential cut-off and the Wien spectrum, following Zdziarski (1985, and references therein). The spectral slope and electron temperature are computed using formulae of Beloborodov (1999a,b). The reprocessed component is not computed. The Comptonized spectrum, $N_{\rm em}$, is normalized to $l_{\rm h}$.

2.2 Effects of photon propagation in Kerr metric

We consider a Kerr black hole characterized by its mass, M, and angular momentum, J. We use the Boyer–Lindquist coordinate

system (t, R, θ, ϕ). The following dimensionless parameters are used below

$$r = \frac{R}{R_{\rm g}}, \qquad \hat{t} = \frac{ct}{R_{\rm g}}, \qquad a = \frac{J}{cR_{\rm g}M}, \qquad \Omega = \frac{{\rm d}\phi}{{\rm d}\hat{t}},$$

where $R_{\rm g} = GM/c^2$ is the gravitational radius. We assume the highest expected value of the spin parameter, $a = 0.998$ (Thorne 1974).

We find the photon number flux observed from a source located at $r_{\rm em}$, $N_{\rm obs}(r_{\rm em})$, by integrating the photon number flux in the source rest frame, $N_{\rm em}$, over all initial directions for which photons reach the observer, and by correcting the photon emission rate by the time dilation factor, ${\rm d}\tau\,/\,{\rm d}t$. Here, ${\rm d}\tau$ and ${\rm d}t$ are time intervals measured in the rest frame and at infinity, respectively (see, for example, Bardeen 1973).

All the photon propagation effects in our model are treated by the transfer function, $\mathcal{T}$, defined by

$$N_{\rm obs}(E,t,i,r_{\rm em}) = \int \mathcal{T}(r_{\rm em},i,g,\Delta\hat{t}) \times N_{\rm em}(E/g, t-\Delta t)\frac{{\rm d}\tau}{{\rm d}t}\,{\rm d}g, \qquad (2)$$

where i is the inclination angle, Δt is the time interval between emission and detection of a given bunch of photons, $\Delta t = \Delta\hat{t}R_{\rm g}/c$, and g is the shift of photon energy, $g = E_{\rm obs}/E_{\rm em}$. Note that the transfer function is independent of M. The only dependence on the black hole mass occurs in the physical scaling of photon travel time and disc area. Then, the total observed spectrum is given by

$$N_{\rm tot}(E,t,i) = \left(\frac{R_{\rm g}}{D}\right)^2 \int_{r_{\rm in}}^{r_{\rm out}} N_{\rm obs}(E,t,i,r)Q(r)2\pi r\,{\rm d}r, \qquad (3)$$

where function $Q(r)$ gives the radial distribution of the emission, $r_{\rm in}$ and $r_{\rm out}$ are the inner and outer radii of the emitting region ($r_{\rm out}$ is fixed at $100R_{\rm g}$) and D is the distance to the source.

We construct the transfer functions following a Monte Carlo method described in detail in Gierliński, Maciołek-Niedźwiecki & Ebisawa (2001). However, Gierliński et al. (2001) consider time-averaged emission, while our model treats time-dependent spectra. Therefore, we extend the procedure to include additional information on the time of photon propagation, as follows.

A large number of photons are emitted from a point source on a Keplerian orbit in the equatorial plane. The angular velocity of the source with respect to the distant observer is

$$\Omega_{\rm K} = \frac{1}{r^{3/2}+a}. \qquad (4)$$

We assume that the source is isotropic and then initial directions of photons are generated from the distribution uniform in both $\phi_{\rm em}$ and $\cos\theta_{\rm em}$, where $\theta_{\rm em}$ is a polar angle between the photon initial direction and the normal to the equatorial plane and $\phi_{\rm em}$ is the azimuthal angle, in the equatorial plane, with respect to the r-direction. Solving the equations of photon motion, as described below, we find the energy shift, inclination and arrival time, $(g, i, \Delta\hat{t})$.

Each element of the transfer function, $\mathcal{T}(r, i, g, \Delta\hat{t})$, is computed by summing all photon trajectories emitted from r for all angles $(\phi_{\rm em}, \theta_{\rm em})$ for which required $(g, i, \Delta\hat{t})$ are obtained.

The travel time and the change of azimuthal angle of a photon emitted at a distance r from the equatorial plane are given by (e.g. Misner, Thorne & Wheeler 1973)

$$\Delta\phi_{\rm ph} = \int_{\pi/2}^{i} \frac{\lambda - a\sin^2\theta}{\Theta^{1/2}\sin^2\theta}{\rm d}\theta + \int_r^D \frac{a(r^2+a^2-\lambda a)}{\Delta\Re^{1/2}}{\rm d}r, \qquad (5)$$

$$\Delta\hat{t}_{\rm ph} = \int_{\pi/2}^{i} \frac{a(\lambda - a\sin^2\theta)}{\Theta^{1/2}}{\rm d}\theta + \int_r^D \frac{(r^2+a^2)(r^2+a^2-\lambda a)}{\Delta\Re^{1/2}}{\rm d}r. \qquad (6)$$

Here, $\Re$ and Θ are, respectively, the radial and polar effective potentials

$$\Re(r) = (r^2+a^2-\lambda a)^2 - \Delta[\xi^2 + (\lambda - a)^2],$$
$$\Theta(\theta) = \xi^2 + \cos^2\theta(a^2 - \lambda^2/\sin^2\theta), \qquad (7)$$

ξ and λ are photon constants of motion, related to the emission angles by

$$\lambda = \frac{\sin\theta_{\rm em}\sin\phi_{\rm em} + V}{(r^2\Delta^{1/2} + 2arV)/A + \Omega_{\rm K}\sin\theta_{\rm em}\sin\phi_{\rm em}},$$
$$\xi = \left(\frac{A}{\Delta}\right)^{1/2}(1-V^2)^{-1/2}(1-\lambda\Omega_{\rm K})\cos\theta_{\rm em}, \qquad (8)$$

$$\Delta = r^2 - 2r + a^2 \qquad (9)$$

$$A = (r^2+a^2)^2 - a^2\Delta \qquad (10)$$

$$V = (\Omega_K - 2ar/A)\frac{A}{r^2\Delta^{1/2}}, \qquad (11)$$

and the angle, i, at which the photon is observed far from the source is determined by the integral equation of motion

$$\int_r^D \Re^{-1/2}{\rm d}r = \int_{\pi/2}^{i} \Theta^{-1/2}{\rm d}\theta. \qquad (12)$$

The shift of energy is given by

$$g = r\left(\frac{\Delta}{A}\right)^{1/2}\frac{(1-V^2)^{1/2}}{1-\Omega_{\rm K}\lambda}. \qquad (13)$$

A photon with trajectory characterized by $\Delta\,\phi_{\rm ph}$ must be emitted when the source is located at $\phi_{\rm s} = \phi_{\rm obs} - \Delta\phi_{\rm ph}$ to reach the observer whose azimuthal angle is $\phi_{\rm obs}$. Then, taking into account $\phi_{\rm s}(t) = \phi_0 + \Omega_K\,t$, where ϕ_0 is a random initial location, we find the arrival time of the photon $\Delta\hat{t} = \Delta\hat{t}_{\rm ph} - \Delta\phi_{\rm ph}/\Omega_K$ for $\Delta\phi_{\rm ph} < 0$ and $\Delta\hat{t} = \Delta\hat{t}_{\rm ph} - (2\pi - \Delta\phi_{\rm ph})/\Omega_K$ for $\Delta\,\phi_{\rm ph} > 0$.

The time dilation factor is given by

$$\frac{{\rm d}\tau}{{\rm d}t} = r\left(\frac{\Delta}{A}\right)^{1/2}(1-V^2)^{1/2}. \qquad (14)$$

The transfer function for a given radius is normalized to the total number of emitted photons. This means that it includes the effect of photon capture by the black hole/accretion disc. This effect suppresses the emission from close to the black hole reaching a distant observer.

Our transfer function is not ideally smooth when plotted, for example, as a function of $\Delta\phi_{\rm ph}$ for a given radius, which is a consequence of finite statistics in the Monte Carlo method. This is apparent in some cases, at the highest frequencies of the PDS.

The sequence of spectra created by the above procedure is subject to standard analysis in the time and Fourier domains (see, for example, van der Klis 1995; Nowak et al. 1999; Poutanen 2001). The power spectra are computed from light curves at 3 keV.

All computations are performed assuming the central black hole mass $M = 10^6\ {\rm M}_\odot$. The parameters of intrinsic variability model are assumed to follow a simple scaling with the black hole mass. That is, their values are adopted as for Cyg X-1 and then scaled by a factor of 10^5

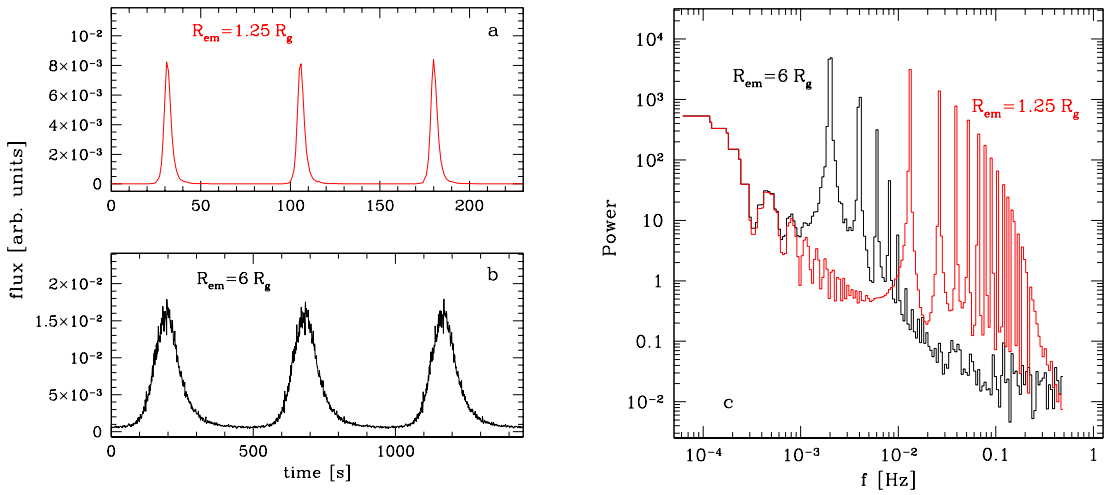

Figure 1. Light curves (a, b) and power spectra (c) from an intrinsically constant signal, modulated by relativistic effects in the Kerr metric with $a = 0.998$. Emission radius is (a) 1.25 R_g and (b) 6 R_g, and disc inclination is 60°. The black hole mass is 10^6 $M_\odot$.

3 RESULTS

The observed flux of radiation from a flare corotating with the disc is periodically modulated. The main contribution to the modulations comes from the Doppler boost; the intensity is modulated as the observed energy of photons varies with their point of emission, so that the invariant I_ν/ν^3 is constant. An additional effect comes from the spectral shape; because $N_{\rm obs}(E)$ contains contributions from $N_{\rm em}(E/g) \propto g^\Gamma E^{-\Gamma}$ (where $\Gamma \sim 1.7$ is the photon spectral index), this enhances the Doppler modulation. Finally, there is also periodic modulation due to varying $\Delta\hat{t}_{\rm ph}$, which influences the time/rate of arrival of photons.

In order to demonstrate the magnitude of the modulation, we plot in Fig. 1 the light curves and power spectra from an intrinsically constant signal emitted at $1.25R_g$ and $6R_g$, and observed at $i = 60°$. The modulation is very strong and non-sinusoidal. For $R_{\rm em} = 1.25R_g$ its amplitude is $\approx 2 \times 10^3$. The non-sinusoidal shape of the modulation means that the PDS contains strong harmonics – peaks at multiples of the fundamental frequency, $f_0 = T_{\rm orb}^{-1} = (2\pi/\Omega_{\rm K})^{-1}$. The case of $R_{\rm em} = 6R_g$ is qualitatively similar, with the fundamental frequency smaller by factor $\Omega_{\rm K}(6R_g)/\Omega_{\rm K}(1.25R_g) \approx 6.5$. The underlying PDS continuum is approximately a power law $P(f) \propto f^{-2}$, which is a power spectrum of a constant signal for $t > 0$.

Our main results are presented in Fig. 2. The underlying PDS breaks from $\propto f^{-1}$ to $\propto f^{-2}$ at $f_{\rm br} \approx 10^{-5}$ Hz (for a 10^6-$M_\odot$ black hole). Superimposed on this continuum is a strong signal from relativistic modulation. The signal is far from quasi-periodic, both because of the assumed range of radii where the flares are located, and because of the strong harmonic content. For $R_{\rm in} = 6R_g$ the orbital frequency at the inner radius can actually be seen in the PDS, together with two of the higher harmonics. The feature drops sharply

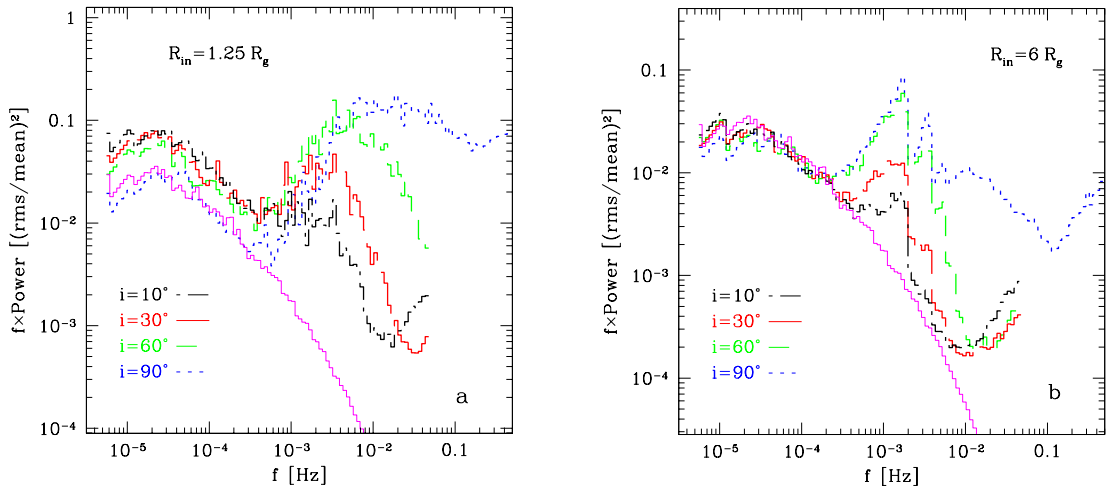

Figure 2. PDS from the flare model, with X-ray flare emission modulated by relativistic effects from Keplerian motion of the flares, in the Kerr metric with $a = 0.998$. The flares are concentrated toward the inner disc radius, so that the radial emissivity follows that expected for an accretion disc in the same metric. The inner disc radius is (a) $R_{\rm in} = 1.25\,R_g$ and (b) $R_{\rm in} = 6\,R_g$. Results for a range of inclination angle, i, are plotted. The PDS for $i = 90°$ is combined from two: one from a light curve with $t_{\rm bin} = 10$ s, and the other with $t_{\rm bin} = 1$ s. The thin solid (magenta online) histograms in both panels show the PDS without the relativistic effects. The black hole mass is 10^6 $M_\odot$. For a BHB system with 10 $M_\odot$, the additional signal appears above 100 Hz.

at $f = T_{\rm orb}^{-1}(R_{\rm in}) \approx 2 \times 10^{-3}$ Hz, while its slope at the low f side is related to the radial distribution of the flares (see Abramowicz et al. 1991). For $R_{\rm in} = 1.25R_{\rm g}$ the relativistic signal in the PDS is quite broad, and the frequency $\Omega_{\rm K}(r = R_{\rm in})$ is not evident there. The main reason for this is again the strong harmonic content, but there are some additional factors. First, the energy dissipation rate dependence on radius, $Q(r)$, goes to zero at $r = R_{\rm ms} \approx R_{\rm in}$. Secondly, both the correction for time units (equation 14) and the fraction of photons escaping to infinity are functions of radius, strongly suppressing the emission from small radii. All these combine to produce the luminosity received from a given radius, $L(r)$, which is peaked at somewhat larger radius than $R_{\rm in}$ (the peak is at $\approx 2R_{\rm g}$). Also, the radial function $L(r)$ is somewhat flatter than r^{-3}.

There is a larger spread in the overall PDS normalization for $R_{\rm in} = 1.25R_{\rm g}$ than for $R_{\rm in} = 6R_{\rm g}$. This is most likely caused by a smaller fraction of flares (thus larger dispersion) contributing to the observed emission for smaller radius. The reason is again that the flares are emitted according to the local energy dissipation rate, $Q(r)$, while in the observed emission the contribution from smallest radii is relatively suppressed.

In the considered frequency range, $10^{-5} < f < 0.05$ Hz, the integrated rms is $\approx$0.09 without the relativistic effects. The additional integrated signal contribution to rms depends, obviously, on $R_{\rm in}$ and i. For $R_{\rm in} = 1.25R_{\rm g}$ it is 0.03–0.40 (see Fig. 2); specifically, it is $\approx$0.06 for $i = 30^\circ$. For $R_{\rm in} = 6R_{\rm g}$ the additional variability rms is in the range 5×10^{-3}–0.11.

For the assumed mass of 10^6 M$_\odot$, the additional signal appears between 10^{-3} and 10^{-2} Hz, i.e. on time-scales of hundreds of seconds. This would correspond to $f > 100$ Hz for a BHB with 10 M$_\odot$.

3.1 Dependence of the strength of the relativistic signal in PDS on radial distribution of flare time-scales

The strength of the relativistic signal in the PDS may depend on assumptions about possible correlations between the radial position of a flare and its time-scale. In our basic model there is no such relation, which means that the probability $P_\tau(\tau_{\rm fl})$ is independent of radius. The relativistic signal is reduced if longer flares occur preferentially at larger distance, because – at a fixed modulation period – the shorter the modulated flare, the lower the quality factor of resulting periodic modulation. We repeat, however, that the simple physically motivated prescription uniquely linking r and $\tau_{\rm fl}$, $\tau_{\rm fl} \propto \Omega_{\rm K}(r)^{-1}$, leads to incorrect radial distribution of emitted energy, which increases with radius (Życki 2002). We have therefore tested more complex r–$\tau_{\rm fl}$ relations. We have modified the radial probability distributions, multiplying the original function, $P_r(r)$, by a Gaussian, $\exp[-(r - r_0)^2/\sigma^2]$, where the centre $r_0 \propto \tau_{\rm fl}^{2/3}$. We have made a number of trial runs with various values of σ, either constant or dependent on r_0. This form of modified probability distribution, $\tilde{P}_r(r)$, indeed favours longer flares to appear farther away from the centre, and the strength of this effect can be controlled by σ. For $\sigma \to \infty$, $\tilde{P}_r(r)$ reduces to original $rQ(r)$, while for $\sigma \to 0$, the unique relation $r_0 \propto \tau_{\rm fl}^{2/3}$ is recovered. Obviously, the above form of $\tilde{P}_r(r)$ is completely arbitrary; its only purpose is to test the dependence of our results on possible unknown relation r–$\tau_{\rm fl}$.

Fig. 3 shows examples of PDS and radial distributions of emission for such modified probability distributions. The dotted (red online) histograms show a case of strong correlation between r and $\tau_{\rm fl}$, with $\sigma = 0.2\, r_0$. This results in energy emission shifted towards larger radii and, in consequence, no relativistic signal in PDS. The dashed (green online) histograms show results for $\sigma/r_0 = 0.2 + 0.4\, \ln(\tau_{\rm fl}/\tau_{\rm min})/\ln(\tau_{\rm max}/\tau_{\rm min})$, meaning a narrow radial distribution for short-lived flares, which progressively becomes broader for longer flares. This gives the emissivity somewhat shifted to larger r and weaker quasi-periodic oscillation (QPO) signal compared to the basic unmodified model. However, when the function $P_r(r)$ is now modified to be a steeper function of r, so that the radial emissivity is restored to its original dependence, $rQ(r)$, the strength of the QPO signal is also restored (the flares are moved closer to the centre).

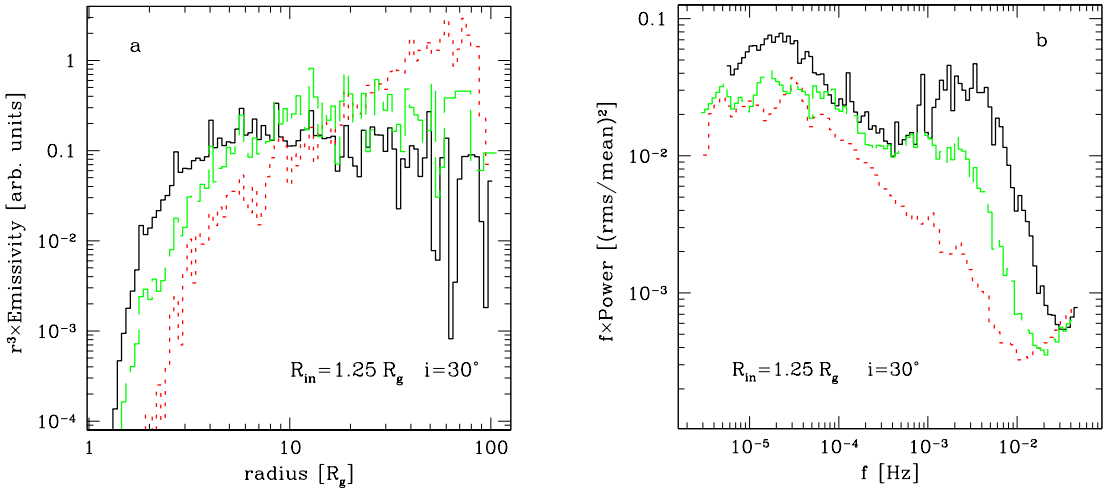

Figure 3. Examples of modified radial probability distribution of flares, with resulting radial emissivities (a) and PDS (b). In the modified models, longer flares occur preferentially at a large distance, as expected from physical arguments (see Section 3.1). The emissivities were multiplied by r^3 (asymptotically, $Q(r) \propto r^{-3}$). Solid (black online) histograms show the original model for $R_{\rm in} = 1.25R_{\rm g}$ and $i = 30^\circ$ as a reference. Dotted (red online) histograms show a model with strong correlation between r and $\tau_{\rm fl}$, resulting in the emissivity peaking at large r and lack of the relativistic signal in PDS. Dashed (green online) histograms demonstrate a case of relatively narrow radial distribution of short-lived flares, while the radial distribution of longer flares becomes progressively broader. When the radial emissivity is forced to have a given steep radial dependence, the strength of the relativistic signal in PDS is independent of any r–$\tau_{\rm fl}$ relation.

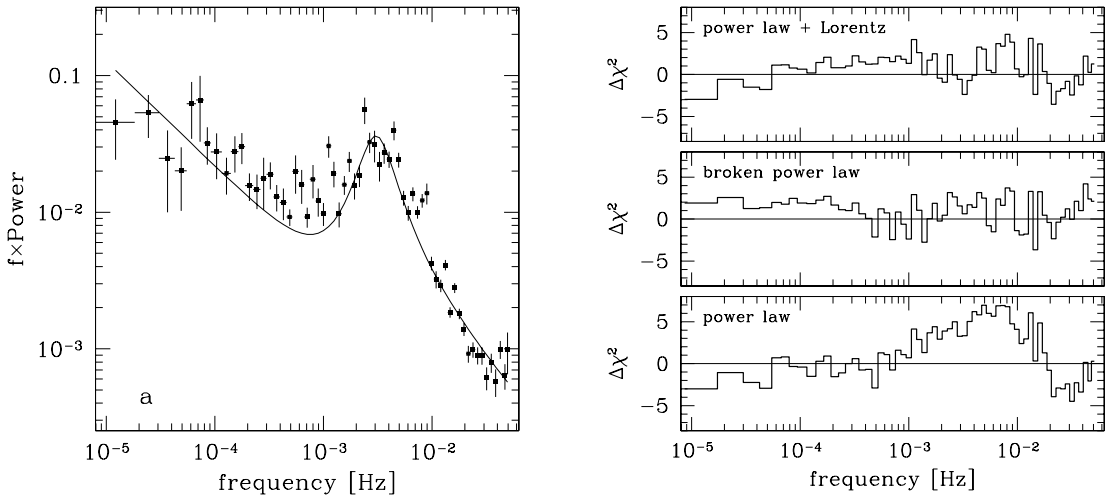

Figure 4. The relativistic signal can be easily seen in PDS from high-quality *XMM–Newton* data of MCG–6-30-15. The model light curve for $R_{\rm in} = 1.25R_{\rm g}$ and $i = 30^\circ$ (see Fig. 2a) was used to generate a light curve of quality corresponding to the observations of Vaughan et al. (2003). The total length of the light curve is $\approx 4 \times 10^5$ s, the mean count rate is 20 cts s^{-1}, and the time bin is 10 s. (a) shows the resulting PDS with Poisson level subtracted, and with a best-fitting power law plus a Lorentzian model. The right panels show the data–model residuals. The additional signal in PDS is highly significant, although its detailed description is not unique. No such signal is seen in the actual data of that Seyfert galaxy (see figs 4 and 5 in Vaughan et al. 2003).

Concluding, when the radial emissivity is forced to have a prescribed form, the (unknown) relation between radial position and lifetime of a flare does not seem to have any influence on the strength of the relativistic signal in the PDS. We do note that this requires that some longer flares occur close to the centre, in apparent contradiction with the basic condition that the flare time-scale should be of the order of the Keplerian time-scale (e.g. Romanova et al. 1998).

4 DISCUSSION

The broad Fe Kα lines and reflection spectra observed in X-ray data of many accreting black holes imply fast Keplerian rotation of the reprocessing matter, but they do not imply that the sources of primary radiation participate in this motion. Moreover, the primary spectra, being of an approximately power-law form, are not expected to be distorted by the relativistic effects. Therefore, we have computed timing signatures of these relativistic effects on primary Comptonized emission. We have assumed that the basic form of variability PDS is a result of a flare avalanche model of PF99 and that the flares correspond to compact sources corotating with the Keplerian accretion disc. We have estimated the position and strength of the additional signal in the PDS due to periodic modulation of intensity from the Doppler and other effects. We now discuss briefly the applicability of our results to current data of Seyfert galaxies and BHB systems.

4.1 Seyfert galaxies

The Seyfert 1 galaxy MCG–6-30-15 is the best example of an AGN with a broad Fe Kα line. The line profile in this source apparently requires X-ray reprocessing to take place very close to the horizon of a rapidly rotating black hole (e.g. Fabian et al. 2002, and references therein). If the sources of primary emission participate in the Keplerian emission, this would produce very clear timing signatures. In order to see whether they would be observable in current data, we simulate a light curve corresponding to the recent *XMM–Newton* observations described by Vaughan et al. (2003). We use the unmodified model, i.e. without any r–$\tau_{\rm fl}$ correlation (Section 3.1), because it ensures the steep radial emissivity, as required by the Fe line profile fits. The model light curve, $F(t)$, is scaled to a given mean value, μ. The 'observed' light curve is then formed by drawing a number of counts in each time bin from the Poisson distribution of mean $F(t_{\rm n})$, where $t_{\rm n} = n \times t_{\rm bin}$, $n = 1, 2, \ldots, N$. Thus, the simulated light curve contains the effect of Poisson noise. The time bin is $t_{\rm bin} = 10$ s, the total duration of the light curve is $\approx 10^5$ s, while the mean value, $\mu = 20$ cts s^{-1}, all as in actual observations (see fig. 1 in Vaughan et al. 2003). Fig. 4 shows the resulting PDS with the Poisson noise level subtracted, together with a best-fitting power law plus Lorentzian model. A simple power-law model gives a bad fit to the data, $\chi^2_\nu = 747/61$ d.o.f. Improvement by adding the Lorentzian is significant, $\chi^2_\nu = 257/58$ d.o.f., although the description of the additional feature in the PDS is not unique; a broken power-law model gives a fit of the same quality. We have checked that a similarly significant difference between the two model fits to the PDS with relativistic effects is maintained, even if the mean source count rate is four times lower. Thus, the signal from relativistic modulation, if present, could be observable, in current data. The signal is, however, not observed (see figs 4 and 5 in Vaughan et al. 2003). The lack of the signal is problematic for the model of rotating flares, suggesting alternative geometries, which do not require Keplerian motion of the X-ray sources.

On the other hand, the periodically variable redshifted Fe Kα line was recently reported in *XMM–Newton* data of NGC 3516 by Iwasawa, Miniutti & Fabian (2004). The variability could be interpreted as a result of the Doppler effect from a flare corotating with a disc, with orbital period $\approx$25 ks. Because this kind of transient modulated line emission is not expected from a model with axially symmetric illumination, this observation provides an argument in favour of the rotating source model. However, the primary continuum does not show the expected modulation. These two observational results – modulation of the Fe Kα line and lack of modulation of the primary continuum – if firmly established, will certainly require revision of current X-ray emission models.

One obvious consequence of the relativistic modulation is that highly inclined sources should show stronger modulation than less inclined sources. This was also pointed out by Czerny et al. (2004) for Seyfert 1 versus Seyfert 2 galaxies. This effect may not be easily observable, however, if the geometry of accretion in Seyfert galaxies corresponds to the low state of BHBs, and the accretion discs are truncated far from the last stable orbit. Because the strength of the relativistic signal decreases very quickly with increasing inner disc radius, these effects can only be observed in sources in high states where the disc extends all the way to the last stable orbit.

4.2 Black hole binaries/other objects

Two BHBs were reported to have very broad Fe Kα lines in their *XMM–Newton* spectra: GX 339−4 (Miller et al. 2004) and GRO J1650−500 (Miller et al. 2002). The inner disc radius inferred from the fits to the line profiles are 2–3$R_{\rm g}$, similar to that in MCG–6-30-15. Thus, in principle, high-frequency PDS should contain the signal due to relativistic modulation. However, as is well known, stellar-mass black hole systems are less suitable to investigating short time-scale variability than AGNs; even though their X-ray fluxes are $\sim 10^3$ times higher than from AGNs, the required time-scales are 10^5–10^7 times shorter. Our simulations indicate that it would be rather difficult to detect the additional signal above 100 Hz. On the other hand, high-frequency QPOs are observed in power spectra of X-ray binaries. Some of these QPOs are located at high frequencies, $f >$ 100 Hz, i.e. in a region where the signal from relativistic modulations might appear (see, for example, Schnittman & Bertschinger 2004). It is rather uncertain, however, how this mechanism might explain the observed QPO, because it would require modulation from a narrow ring of the disc, and suppression of the harmonics, in order to produce a narrow QPO feature.

5 CONCLUSION

Keplerian motion of sources of X-ray radiation in accreting black holes gives a very strong signature in power spectra, if the sources are located close to the centre. Such a signal, if present, would be observed in recent high-quality data, for example, the *XMM–Newton* data from the Seyfert 1 galaxy MCG–6-30-15. Lack of the signal in these data poses problems for models assuming that the X-ray sources participate in the Keplerian disc motion, as for example expected for magnetic flares.

ACKNOWLEDGMENTS

We thank Chris Done and Kris Beckwith for discussions on relativistic effects. This work was partly supported by grants nos. 2P03D01225 and PBZ-KBN-054/P03/2001 from the Polish State Committee for Scientific Research (KBN).

REFERENCES

Abramowicz M. A., Bao G., Lanza A., Zhang X.-H., 1991, A&A, 245, 454
Bao G., 1992, A&A, 257, 594
Bao G., Ostgaard E., 1995, ApJ, 443, 54
Bardeen J. M., 1973, in DeWitt C., DeWitt B. S., eds, Black Holes. Gordon and Breach, New York, p. 215
Bardeen J. M., Cunningham C. T., 1973, ApJ, 183, 237
Beloborodov A. M., 1999a, ApJ, 510, L123
Beloborodov A. M., 1999b, in Poutanen J., Svensson R., eds, ASP Conf. Ser. Vol. 161, High Energy Processes in Accreting Black Holes. Astron. Soc. Pac., San Francisco, p. 295 (astro-ph/9901108)
Churazov E., Gilfanov M., Revnivtsev M., 2001, MNRAS, 321, 759
Cunningham C. T., Bardeen J. M., 1972, ApJ, 173 L137
Czerny B., Nikołajuk M., Piasecki M., Kuraszkiewicz J., 2001, MNRAS, 325, 865
Czerny B., Różańska A., Dovčiak M., Karas V., Dumont A.-M., 2004, A&A, 420, 1
Done C., 2002, Phil. Trans. R. Soc., 360, 1967 (astro-ph/0203246)
Fabian A. C. et al., 2002, MNRAS, 335, L1
Galeev A. A., Rosner R., Vaiana G. S., 1979, ApJ, 229, 318
Gierliński M., Maciołek-Niedźwiecki A., Ebisawa K., 2001, MNRAS, 325, 1253
Iwasawa K., Miniutti G., Fabian A. C., 2004, MNRAS, 355, 1073
Krolik J. H., 1999, Active Galactic Nuclei. Princeton Univ. Press, Princeton, NJ
Maccarone T. J., Coppi P. S., Poutanen J., 2000, ApJ, 537, L107
McHardy I. M., Papadakis I. E., Uttley P., Page M. J., Mason K. O., 2004, MNRAS, 348, 783
Markowitz A. et al., 2003, ApJ, 593, 96
Miller J. M. et al., 2002, ApJ, 570, L69
Miller J. M. et al., 2004, ApJ, 606, L131
Miniutti G., Fabian A. C., 2004, MNRAS, 349, 1435
Misner C. W., Thorne K. S., Wheeler J. A., 1973, Gravitation. W. H. Freeman, San Francisco
Nowak M. A., Wilms J., Vaughan B. A., Dove J. B., Begelman M. C., 1999, ApJ, 515, 726
Poutanen J., 2001, Adv. Space Res., 28, 267 (astro-ph/0102325)
Poutanen J., Fabian A. C., 1999, MNRAS, 306, L31 (PF99)
Reynolds C. S., Nowak M. A., 2003, Phys. Rep., 377, 389
Romanova M. M., Ustyugova G. V., Koldoba A. V., Chechetkin V. M., Lovelace R. V. E., 1998, ApJ, 500, 703
Schnittman J. D., Bertschinger E., 2004, ApJ, 606, 1098
Thorne K. S., 1974, ApJ, 191, 507
Turner N. J., 2004, ApJ, 605, L45
van der Klis M., 1995, in Lewin W. H. G., van Paradijs J., van den Heuvel E. P. J., eds, X-ray Binaries. Cambridge Univ. Press, Cambridge, p. 252
Vaughan S., Fabian A. C., Nandra K., 2003, MNRAS, 339, 1237
Zdziarski A. A., 1985, ApJ, 289, 514
Zdziarski A. A., Gierliński M., 2004, Prog. Theor. Phys. Supp., 155, 99
Życki P. T., 2002, MNRAS, 333, 800

This paper has been typeset from a TEX/LATEX file prepared by the author.